Soft Matter

ROYAL SOCIETY OF CHEMISTRY

PAPER

View Article Online
View Journal

Check for updates

Cite this: DOI: 10.1039/d0sm02023k

CO_2-Driven diffusiophoresis for maintaining a bacteria-free surface†

Suin Shim, *[a] Sepideh Khodaparast, [b] Ching-Yao Lai, [c] Jing Yan, [d] Jesse T. Ault, [e] Bhargav Rallabandi, [f] Orest Shardt [g] and Howard A. Stone *[a]

Received 13th November 2020,
Accepted 18th January 2021

DOI: 10.1039/d0sm02023k

rsc.li/soft-matter-journal

Dissolution and dissociation of CO_2 in an aqueous phase induce diffusiophoretic motion of suspended particles with a nonzero surface charge. We report CO_2-driven diffusiophoresis of colloidal particles and bacterial cells in a circular Hele-Shaw geometry. Combining experiments and model calculations, we identify the characteristic length and time scales of CO_2-driven diffusiophoresis in relation to system dimensions and CO_2 diffusivity. The motion of colloidal particles driven by a CO_2 gradient is characterized by measuring the average velocities of particles as a function of distance from the CO_2 sources. In the same geometrical configurations, we demonstrate that the directional migration of wild-type *V. cholerae* and a mutant lacking flagella, as well as *S. aureus* and *P. aeruginosa*, near a dissolving CO_2 source is diffusiophoresis, not chemotaxis. Such a directional response of the cells to CO_2 (or an ion) concentration gradient shows that diffusiophoresis of bacteria is achieved independent of cell shape, motility and the Gram stain (cell surface structure). Long-time experiments suggest potential applications for bacterial diffusiophoresis to cleaning systems or anti-biofouling surfaces, by reducing the population of the cells near CO_2 sources.

Introduction

The manipulation of colloidal particles and materials can be accomplished using fluid shear and application of external fields (gravity, electric, *etc.*).[1–6] Chemical gradients enable one variant of this particulate-level control, which is generally referred to as diffusiophoresis.[7–12] Experiments and simulations have been reported for many systems, including different electrolytes, geometries, and particle size and type.[13–19] In particular, CO_2-driven diffusiophoresis in an aqueous phase is achieved by dissolution and dissociation of CO_2 and H_2CO_3 in water.[7,11] Due to the large difference in the diffusivity of the two ions (H^+ and HCO_3^-), a large diffusion potential is created and diffusiophoresis of charged particles is achieved with a dominant electrophoretic contribution. One important potential role for a chemical gradient is the controlled migration of bacteria, as the bacterial cells have a negative surface charge.[20,21] We investigate this topic, show that CO_2-driven diffusiophoresis can produce a bacteria-free zone near a surface exposed to dissolved carbon dioxide, and so suggest new routes for reducing bacterial density, and potentially biofilm formation, at surfaces.

Here we use a circular Hele-Shaw geometry with either a CO_2 bubble[22–24] or a CO_2-pressurized chamber to investigate the transport of polystyrene particles and bacterial cells. Combining experiments and model calculations, we understand the characteristic length and time scales of CO_2-driven diffusiophoresis in relation to the system dimensions and CO_2 diffusivity. We then study motion of wild-type *Vibrio cholerae* and a mutant lacking flagella (Δ*flaA*) near a dissolving CO_2 source, and show that the directional motion is diffusiophoresis, not CO_2-driven *chemotaxis*. Also, our experiments with *Staphylococcus aureus* and *Pseudomonas aeruginosa* show that diffusiophoresis driven by CO_2 dissolution can be achieved for both Gram-positive and Gram-negative bacteria, independent of cell shape. Diffusiophoresis of motile bacterial cells is not identical to that of colloidal particles or immotile cells. We report that the motile bacteria maintain their characteristic swimming speed and show a slow drift in the radially-outward direction due to diffusiophoresis, with an estimate for the Péclet number $Pe \approx 10^{-3}$–10^{-2}.

[a] Department of Mechanical and Aerospace Engineering, Princeton University, Princeton, NJ 08544, USA. E-mail: sshim@princeton.edu, hastone@princeton.edu
[b] School of Mechanical Engineering, University of Leeds, Leeds LS2 9JT, UK
[c] Department of Geosciences, Princeton University, Princeton, NJ 08544, USA
[d] Department of Molecular, Cellular and Developmental Biology, Quantitative Biology Institute, Yale University, New Haven, CT, 06511, USA
[e] School of Engineering, Brown University, Providence, Rhode Island 02912, USA
[f] Department of Mechanical Engineering, University of California, Riverside, California 92521, USA
[g] Bernal Institute and School of Engineering, University of Limerick, Castletroy, Limerick, V94 T9PX, Ireland

† Electronic supplementary information (ESI) available. See DOI: 10.1039/d0sm02023k

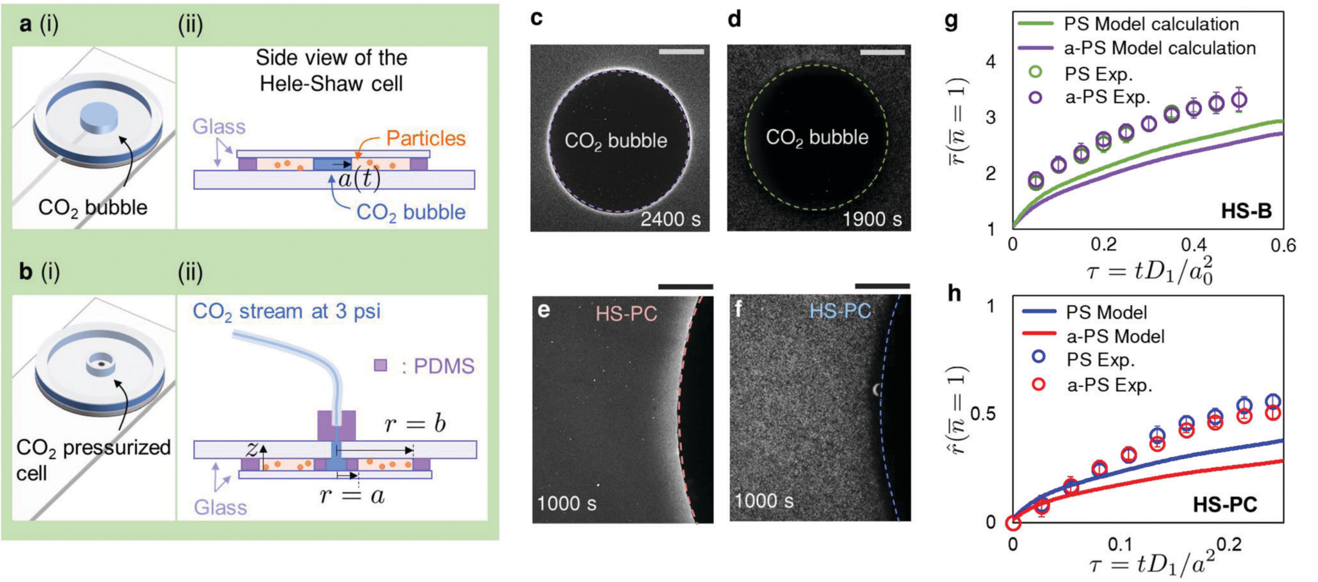

Fig. 1 CO_2-driven diffusiophoresis of colloidal particles. (a and b) Schematics of experimental setup for (a) HS-B and (b) HS-PC. See ESI† for details. (c and d) Charged particles near a dissolving CO_2 bubble (HS-B). Distribution of (c) amine-modified polystyrene (a-PS) particles and (d) polystyrene (PS) particles show, respectively, local accumulation and exclusion of charged particles by diffusiophoresis. Bright dots indicate particles. (e and f) Charged particles near the CO_2 source in HS-PC. Distribution of (e) a-PS and (f) PS particles near the fixed CO_2 source show local accumulation and exclusion. (g and h) Comparison between experimental measurements and model calculations (ESI†) of the macroscopic growth of the accumulation and exclusion zones. (g) Measured and calculated values of $\bar{r}(\bar{n} = 1)$ are plotted *versus* τ for HS-B. (h) Measured and calculated values of $\hat{r}(\bar{n} = 1)$ are plotted *versus* τ for HS-PC. (g and h) No fitting parameter is used. (c–f) Scale bars are 500 μm.

Finally, we demonstrate that diffusiophoretic migration of *S. aureus* away from the CO_2 source reduces cell adhesion to a surface, and that the exclusion of *P. aeruginosa* lasts ≥11 h after CO_2 is turned off. Thus CO_2-driven diffusiophoresis can prevent surface contamination or infection by reducing the population of cells approaching an interface, and the CO_2-enabled reduction of bacterial cell density near a surface can be applied to liquid cleaning systems and anti-biofouling surfaces.

Results

When an aqueous suspension of charged colloidal particles is exposed to dissolving CO_2, positively (negatively) charged particles migrate toward (away from) the CO_2 source by diffusiophoresis;[7,11] the fast diffusing H^+ relative to HCO_3^- from the dissociation of H_2CO_3 drives the transport. The diffusivity of CO_2 molecules and the ambipolar diffusivity of the ions are, respectively, $D_1 = 1.91 \times 10^{-9}$ m^2 s^{-1} and $D_A = 2.1 \times 10^{-9}$ m^2 s^{-1}.[25] We investigate the phenomenon using a Hele-Shaw geometry (Fig. 1; a circular cell with radius b = 11 mm and height h = 500 μm). Here, diffusiophoresis near a CO_2 source is documented experimentally and calculated (ESI†) for two configurations – a dissolving CO_2 bubble (Fig. 1(a); we call this system HS-B) and a CO_2-pressurized chamber (Fig. 1(b); HS-PC) – to examine both moving and fixed boundaries. We provide scaling arguments in the derivation of the model (ESI†) and show that we can assume local chemical equilibrium everywhere in our system. Such condition allows decoupling of the CO_2 diffusion and reaction. Therefore, even though it is the concentration gradient of dissociated ions that drives diffusiophoresis, we choose to use the diffusivity of CO_2 to define the time and velocity scales. The local chemical equilibrium assumption is reasonable as CO_2 dissolves rapidly in water and creates a weak acid; most of the dissolved molecules present in the system are CO_2 (ESI†).

In HS-B, a CO_2 bubble with radius $a(t)$ and an initial radius a_0 dissolves at a typical speed $\frac{\mathrm{d}a}{\mathrm{d}t} \approx \frac{D_1}{a_0} \approx O(0.1 - 1)$ μm s^{-1} until the gas exchange reaches steady state,[7,22–24] where D_1 is the diffusivity of CO_2 in water and a_0 = 2.5–3 mm in our system. A bubble reaches its steady state within a nondimensional time $\tau = \frac{t}{a_0{}^2/D_1} \approx 1$ (≈1 h; ESI†). The typical diffusiophoretic

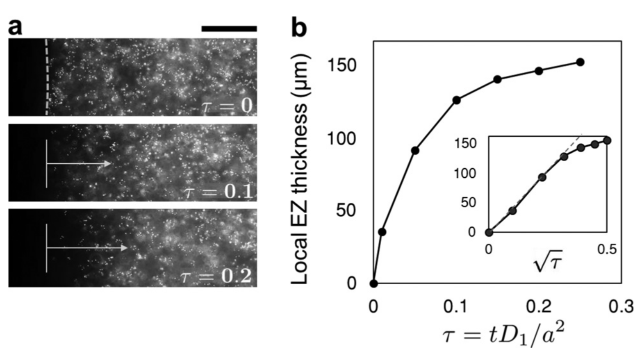

Fig. 2 Growth of local exclusion zone (EZ) in HS-PC system. (a) Images showing exclusion of PS particles near the PDMS wall. Scale bar is 100 μm. (b) Growth of EZ plotted *versus* nondimensional time. Inset: Growth of EZ plotted *versus* $\sqrt{\tau}$ showing early dependence on $\sqrt{t}$.

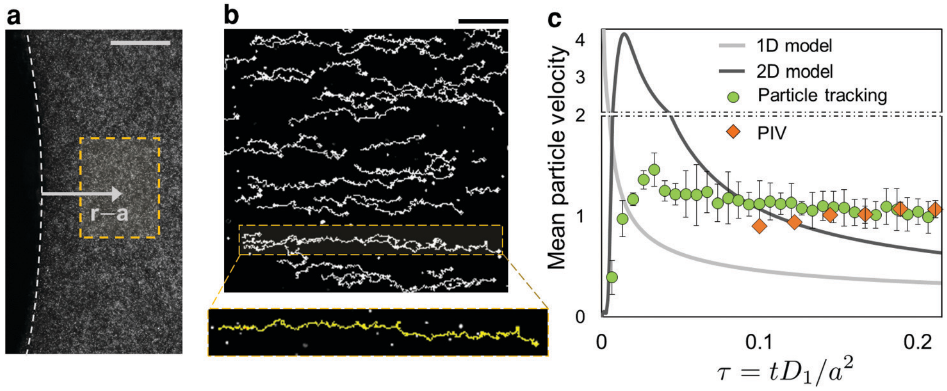

Fig. 3 Velocity measurements for the PS particles. (a) Image showing the fixed boundary and a measurement window for PIV and particle tracking in HS-PC. (b) Images visualizing particle trajectories that are longer than 60 frames (1 min). Bright dots are PS particles. (c) Mean particle (radial) velocities from the PIV and particle tracking are plotted *versus* nondimensional time and compared with the model calculations. All velocities are nondimensionalized with D_1/a. Scale bars are, (a) 300 μm and (b) 50 μm.

velocity of nearby suspended particles $u_p = \Gamma_p \nabla \ln c_i$ scales as $u_p \approx \frac{\Gamma_p}{a_0} \approx O(0.1-1)\ \mu m\ s^{-1}$, where Γ_p and c_i are the diffusiophoretic mobility of particles and concentration of ions, respectively (ESI,† Video 1). The relative motion of particles and the interfaces creates a charge-dependent particle distribution for both HS-B and HS-PC (Fig. 1(c–f)). The radius of the inner chamber (where CO_2 is pressurized) in HS-PC is a = 3 mm, and we use this as the characteristic length scale for HS-PC experiments.

Locally, in the vicinity of the interface, amine-modified polystyrene (a-PS, positively charged, diameter = 1 μm) particles accumulate and form a high particle-density region, whereas polystyrene (PS, negatively charged, diameter = 1 μm) particles create an exclusion zone (EZ; Fig. 1(c–f)), where the particle concentration is small. Growth of the local EZ in HS-PC (Fig. 2 and ESI†) is proportional to $\sqrt{t}$, similar to EZ formation near an ion-exchange membrane.[10]

Particle accumulation and exclusion also occur on the length scale $\ell \approx a_0$ (or $\ell \approx a$) in both systems (Videos S2 and S3, ESI†). In the one-dimensional model we define the boundaries of such macroscopic accumulation and exclusion as the radial distance where the nondimensional particle concentration $\bar{n} = n/n_0 = 1$ ($n(r,t)$ is the particle concentration and $n_0 = n(r,0)$; ESI†). The nondimensional radial positions are defined as $\bar{r} = r/a_0$ for HS-B, and $\hat{r} = \frac{r-a}{b-a}$ for HS-PC. Such boundaries are determined analogously in the experiments (ESI†) and plotted *versus* τ in Fig. 1(g and h). Both systems show consistent trends in the growth of macroscopic boundaries (Fig. 1(g and h)). In HS-B, the measured boundaries are larger than in the one-dimensional model from the beginning due to the initial rapid generation of the bubble, which is not included in the model calculation. Bubble generation introduces fast interface growth, which enhances CO_2 dissolution at early times and causes faster diffusiophoresis.

The macroscopic boundaries increase up to almost half of the radius of the Hele-Shaw cell ($\approx 0.5b$) within τ = 0.2 in HS-PC (Fig. 1(h)). In HS-B, as noted from the time evolution of the radius (ESI†), there is a velocity contribution from the shrinking bubble (da/dt) that affects the particle distribution, and this effect lasts up to $\tau \approx 1$.

The diffusiophoretic velocities of PS particles in HS-PC can be analyzed further. We selected a measurement window of width = 400 μm and height = 500 μm at a fixed position (Fig. 3(a); 200 μm away from the wall. All images are obtained at $z = h/2$ = 250 μm of the Hele-Shaw cell). Then we obtained the average velocities of PS particles using particle tracking and particle image velocimetry (PIV) (see Methods for details). Particle trajectories were analyzed with a set of fluorescent images taken every 1 s, and the 1 minute-average of the radial velocities are plotted *versus* time (Fig. 3(b and c)). The radial velocities are also calculated from one- and two-dimensional models, and plotted *versus* time for comparison (see ESI† for details); all velocities are nondimensionalized with D_1/a. The one-dimensional (1D) model approximates the Hele-Shaw cell as a disk and solves for radial diffusiophoresis near a dissolving CO_2 bubble or a fixed CO_2 chamber. The two-dimensional (2D) model considers a side-view of the Hele-Shaw cell and solves the radial motion of particles under the influence of the diffusioosmotic slip at the top and bottom walls. In the 1D model, we use a constant CO_2 concentration as the boundary condition, and the diffusiophoretic velocity (= $\Gamma_p \nabla \ln c_i$) is largest at t = 0 due to the sharp concentration gradient. In the 2D model, we used the time-dependent boundary condition for CO_2 concentration (ESI†), to include the diffusion of CO_2 through the PDMS wall. As a result, we obtain an increase then decrease of particle velocities at early time (Fig. 3(c)). A similar trend is observed in the particle tracking analysis, where the nondimensional radial velocity of particles increases up to ≈ 1.5 (Fig. 3(c)), then slowly decreases to ≈ 1. As the diffusiophoretic motion of particles develops over time, spatiotemporal variation of the velocities is expected to decrease in the measurement window and the velocimetry can be done for the collective migration, employing PIV.

We denote the distance of the far side of the measurement window from the edge of the CO_2-pressurized chamber by

$r - a = \ell_w$ (= 600 μm). Then, we note that the characteristic dimensionless time $\tau = 0.1 = 2.5\tau_{w1}$, where $\tau_{w1} = \frac{\ell_w{}^2/D_1}{a^2/D_1}$, which is the time needed for CO_2 to diffuse ℓ_w. Also, the experimental measurements show that the average particle velocity in the measurement window is $u_w \approx D_1/a \approx 0.7$ μm s^{-1} (Fig. 3(c)). For the particles, it takes them $\tau_{w2} = \frac{\ell_w/u_w}{a^2/D_1}$, so $\tau \approx 0.2$ to travel the distance ℓ_w. From these scaling estimates, we can conclude that $\tau \approx 0.1$ is the time required for the ion concentration field and the radial diffusiophoretic motion of particles to develop in the region of analysis. Beyond this early time ($\tau \gtrsim 0.1$), three-dimensional complexity near the CO_2 source is expected to decrease (ESI†), and we can stably measure the radial velocity of PS particles using PIV. We performed particle image velocimetry (PIV) with the image sequence taken every 10 s, and the 100 second-average of the velocity vectors are plotted *versus* time (Fig. 3(c)). For further experiments with bacteria, we report spatially resolved PIV measurements obtained for $\tau > 0.1$ to characterize the diffusiophoresis.

Our understanding of the typical length, time and velocity scales of CO_2-driven diffusiophoresis in a Hele-Shaw cell motivated us to extend our investigations to a broader range of particles. Past studies have reported on the use of diffusiphoresis to achieve migration of living cells.[26,27] For example, the goals of particle manipulation can be to clean a region of liquid, achieve antifouling surfaces, or prevent infection in biological systems. Two previous studies report EZ formation in bacterial suspensions in contact with an ion-exchange membrane (Nafion)[28,29] and discuss possible cleaning applications.

CO_2-driven diffusiophoresis of bacteria

As an initial step for demonstrating and investigating diffusiophoresis of bacterial cells by CO_2 dissolution, we chose two types of *V. cholerae* cells – wild-type (WT) and a mutant lacking flagella (Δ*flaA*), both of which are tagged by mKO (monomeric Kusabira Orange), a bright fluorescent protein.[30] We first confirm the diffusiophoretic contribution to the cell transport in the presence of a dissolving CO_2 source in a Hele-Shaw geometry. Then, using PIV, we measure the velocities of the bacterial cells that move along the ion concentration gradient.

V. cholerae is Gram-negative, comma-shaped (length ≈ 2–3 μm, diameter ≈ 1 μm), and single flagellated. The net surface charge of *V. cholerae* (as well as other bacteria) is negative,[31,32] so the cells are expected to migrate away from a CO_2 source by diffusiophoresis (Video S4, ESI†). We prepared a bacterial solution by diluting the growth suspension (Methods) to 10% M9 minimal salt solution. No nutrient is provided so no growth and division occur on the time scale of the experiment. Using low salt concentration helps to exclude the effects of coupled ion fluxes on the diffusiophoresis of bacteria.[33] Similar to the particle experiments, we fill the Hele-Shaw cell with bacterial suspension, and introduce either a CO_2 bubble or pressurize CO_2 in the inner chamber. Fluorescence intensities near the CO_2 source for both HS-B and HS-PC systems are measured

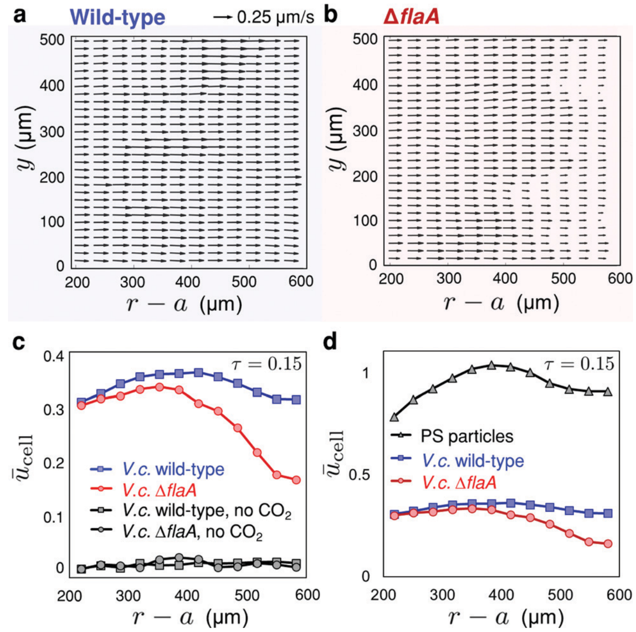

Fig. 4 Velocity measurements for CO_2-driven diffusiophoresis of *V. cholerae*. (a and b) PIV for *V. cholerae* cells in the HS-PC experiments. Velocity vectors plotted *versus* position ($r - a$, y). Motion of (a) wild-type and (b) Δ*flaA* cells at $t \approx 10$ minutes. The directional motion of cells is described by aligned velocity vectors in the radially outward direction. (c) Nondimensional y-averaged velocities obtained from (a and b) and control experiments without CO_2 at $\tau = 0.15$ (≈10 minutes) plotted *versus* $r - a$. (d) Nondimensional y-averaged velocities of PS particles, WT and Δ*flaA* cells obtained at $\tau = 0.15$ plotted *versus* $r - a$.

(ESI† Fig. S13), and the intensity change shows that the cell number near the dissolving CO_2 source decreased significantly over time.

Similar to the PS particles, the use of PIV near the fixed boundary allows us to measure the diffusiophoretic velocity of the cells by a dissolving CO_2 source. We plotted the velocity vectors *versus* position in Fig. 4(a and b), where the origin of the y-axis is at the bottom left corner of the measurement window. After the CO_2 valve is opened at $\tau = 0$, both strains of *V. cholerae* migrate radially outward (Fig. 4(a and b)). The radial alignment of the velocity vectors confirms that both motile and immotile *V. cholerae* cells move along the CO_2-generated ion concentration gradient. In Fig. 4(c), nondimensional velocities ($\bar{u}_{cell} = u_{cell}/(D_1/a)$; u_{cell} is the y-average of the measured velocity) of the cells at $\tau = 0.15$ with and without dissolving CO_2 are plotted *versus* radial position. Our observation that both motile and immotile cells exhibit directional movement with similar velocities shows that the motion is not a chemotactic effect. If the motion is CO_2-driven chemotaxis, the Δ*flaA* strain should not migrate under the concentration gradient. We also compare the typical velocity scales of the cells and the PS particles in Fig. 4(d). The diffusiophoretic velocity of the bacterial cells is smaller than that of the PS particles, and as a first rationalization, this is due to the smaller diffusiophoretic mobility of the cells. Our comparison suggests that the *V. cholerae* cells have three to four times smaller mobility compared to the PS particles, since the diffusiophoretic velocity scales as $u_p \approx \frac{\Gamma_p}{a}$.

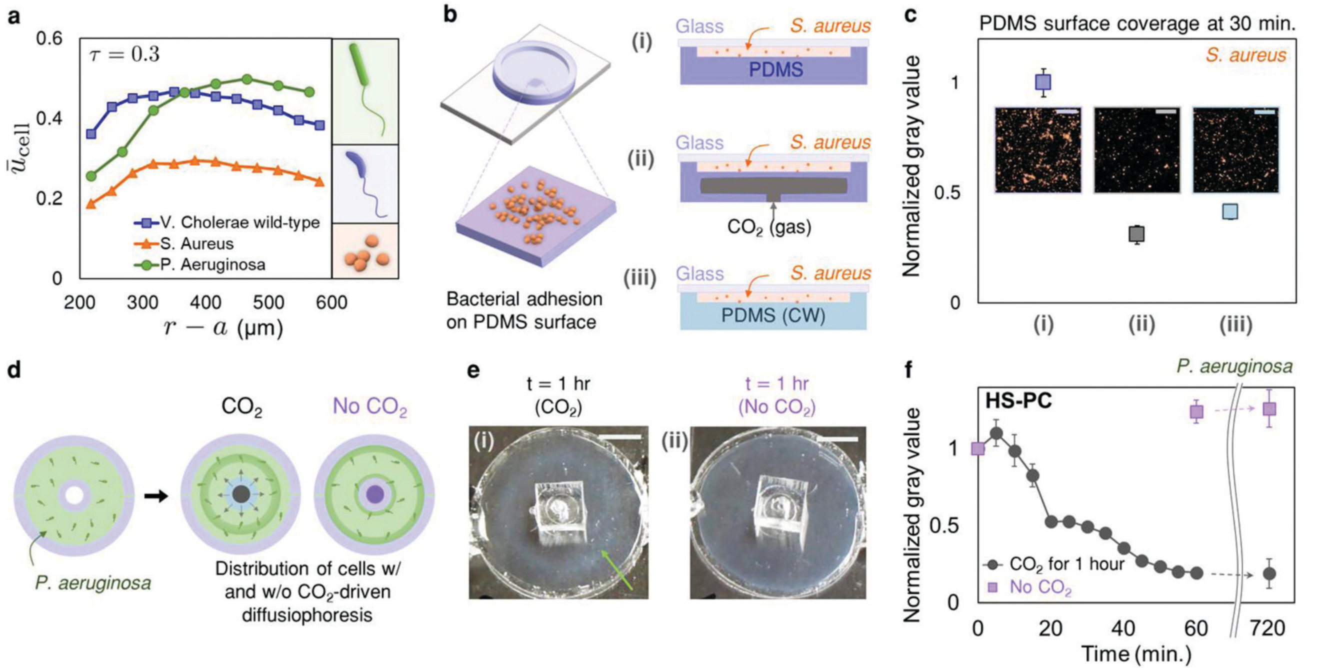

Fig. 5 CO_2-driven diffusiophoresis of *S. aureus* and *P. aeruginosa*. (a) Velocity measurements of bacterial cells near the CO_2 source (fixed boundary configuration) at $\tau = 0.3$ ($t \approx 20$ min). Right panels: schematics showing cell shape. (b) Schematics of surface coverage experiments for *S. aureus* cells on PDMS surfaces. We tested three scenarios: (b-i) plain PDMS substrate in ambient air, (b-ii) pressurized CO_2 gas under the PDMS substrate, and (b-iii) PDMS substrate that is saturated with carbonated water (CW). (c) Intensity measurements for cell coverage on PDMS substrate at $t = 30$ min. The gray values are normalized by that of a corresponding no-CO_2 experiment. Inset images show surface coverage of *S. aureus* cells on three different PDMS surfaces. (d–f) Long time effect of diffusiophoresis: diffusiophoresis of *P. aeruginosa* cells in the fixed boundary system. (d) Schematic of two control experiments in the fixed boundary configuration. In the presence of a finite-time CO_2 source, cells move radially outward and form an accumulation front (ring structure) in the chamber. On the other hand, when the CO_2 source is replaced by an air source, cells gradually concentrate toward both PDMS walls. (e-i and ii) Images showing the Hele-Shaw chamber at $t = 1$ h. (f) Fluorescent intensity measurements near the CO_2 source for two experiments in (d and e). Accumulation and exclusion of bacterial cells near the inner PDMS wall is maintained up to 12 hours, proving the long-term effect of diffusiophoresis. Scale bars are (c) 50 µm, and (e) 5 mm.

For both wild-type and immotile *V. cholerae*, we use PIV to measure the diffusiophoretic velocities ≈ 0.3 µm s^{-1} (Fig. 4(a and b)) at $\tau = 0.15$. This value is much smaller than the typical swimming speed of motile *V. cholerae* (≈ 30 µm s^{-1}; ESI†). Our observations of diffusiophoresis of motile bacteria are that the cells maintain their swimming behavior randomly in all directions, with a slow (radial) drift in the Hele-Shaw cell, following the ion concentration gradient. We interpret the difference in the PIV profiles between the two strains as due to the motility of the wild type cells. Detailed discussions including the effective diffusivity of the motile bacteria are presented in the last section.

To highlight the generality of the phenomenon, two more bacteria were examined – *S. aureus* (mKO labeled, Gram-positive, spherical and immotile)[34] and *P. aeruginosa* (mCherry labeled, Gram-negative, rod shaped and motile)[35] for their diffusiophoretic response to dissolving CO_2 (Fig. 5). For the HS-PC system, the measured velocities ($\bar{u}_{cell}$) at $\tau = 0.3$ are plotted *versus* $r - a$ in Fig. 5(a). We note that *S. aureus* is slower compared to the other two bacteria. Both *S. aureus* and *P. aeruginosa* have surface zeta potentials $\zeta \approx -30$ mV,[36–38] so the velocity difference is unexpected given that electrophoresis makes the dominant contribution to CO_2-driven diffusiophoresis, where Γ_p is a function of ζ[9] (ESI†). One feature of *S. aureus* is that surface adhesive proteins[39] make the cells easily form clusters, which may contribute to the change in the diffusiophoretic velocity and larger clusters are consistent with the slower diffusiophoretic speeds.[15,40] Also, different diffusiophoretic velocities may arise from different shapes of the cells (Fig. 5(a)). *S. aureus* is approximately spherical with a diameter ≈ 1 µm, while *P. aeruginosa* is ≈ 1–5 µm long and ≈ 0.5–1 µm in diameter. Assuming similar ζ for the three bacteria and the largest aspect ratio for *P. aeruginosa*, we obtain an aspect-ratio dependence of the diffusiophoretic velocities of the cells.[41] Our results also show that the surface zeta potential is not the only parameter for determining the diffusiophoretic velocity of bacterial cells.

In order to move toward applications for diffusiophoretic bacterial removal using CO_2, we first quantify the surface coverage of *S. aureus* cells to surfaces under different CO_2 dissolution conditions. Fig. 5(b) illustrates three conditions of PDMS substrates (b-i) without and (b-ii and iii) with CO_2 sources. CO_2 is introduced either by pressurizing CO_2 below a PDMS membrane or by saturating PDMS with carbonated water (CW; Methods). Then the surface coverage 30 minutes after injection of a *S. aureus* suspension into the chamber above the PDMS substrate was measured by the fluorescent intensity (Fig. 5(c)). We observe that the surface coverage of *S. aureus* is significantly decreased in the presence of CO_2, and this is evidence that the CO_2-generated ion concentration gradient removed the cells from the vicinity of the substrate, resulting in reduced surface contamination. Below, with a set of experiments with *P. aeruginosa*, we demonstrate that the bacterial removal lasts ≥11 hours.

In many discussions of diffusiophoresis, the focus is often on boosting migration of micron-sized particles. This is a clear advantage of the phenomenon, owing to $\Gamma_p \gg D_p$ ($D_p \approx 10^{-13}$ m^2 s^{-1} is the Stokes–Einstein diffusivity of a micron-sized particle). However, smaller particle diffusivity compared to the diffusiophoretic mobility, can also mean that, after eliminating the gradient, the time required for particles to recover their original distribution is long (≈1000 h for 1 μm particles to move 1 mm by diffusion; ESI†).

P. aeruginosa is known for surviving in dilute media[42] for more than 10 days so it is suitable for long-time diffusiophoretic experiments. We performed HS-PC experiments with and without 1 h of CO_2 dissolution in *P. aeruginosa* suspension (Fig. 5(d and e)). We predict and observe that, by CO_2-driven diffusiophoresis, bacterial cells move away from the inner wall, whereas without any CO_2 source, the cells concentrate near both inner and outer PDMS walls where there is an air source. The CO_2 valve was open only for 1 h, but the result of diffusiophoresis lasted longer than 12 hours (Fig. 5(f)). The distribution of the cells at t = 12 h are presented in the ESI.†

Finally, we discuss the diffusiophoresis of *motile* bacteria since it is not identical to that of polystyrene particles or immotile cells of similar size. Both *V. cholerae* and *P. aeruginosa* are single flagellated organisms and exhibit run-reverse patterns.[43] The effective diffusivity of motile bacteria with typical translational speed v_t and reverse time t_r can be estimated as $D_{\mathrm{eff}} \approx v_t^2 t_r \approx O(100)$ μm^2 s^{-1} (ESI†). It is observed (Video S5, ESI†) that the flow of cells under an ion concentration gradient is a slow advection with an estimated Péclet number $\mathrm{Pe} = \frac{u_p \ell_{\mathrm{cell}}}{D_{\mathrm{eff}}} \approx 10^{-3} - 10^{-2}$, where $\ell_{\mathrm{cell}} \approx 1$ μm is the characteristic length of bacterial cells. Cells are observed to swim randomly with their characteristic velocity ≈30–50 μm s^{-1} (ESI†), with a slow drift (radially outward) due to the diffusiophoretic contribution (Video S5, ESI†).

In this article, we demonstrate directed diffusiophoretic migration of colloidal particles and different types of bacteria under a concentration gradient of CO_2, and discuss possible applications of CO_2-driven diffusiophoresis to prevent contamination. For example, delaying biofilm formation can improve the anti-biofouling properties of surfaces. Currently we are working to realize the mechanism at various salt concentrations to broaden the understanding to physiological or higher salinity conditions. Moreover, understanding the characteristic scales and flow structure near the CO_2 source is crucial for the next steps of CO_2-driven diffusiophoresis for mitigating bacterial growth on, or bacterial removal from, surfaces.

Materials and methods

1. Materials and design

The Hele-Shaw cell is made by placing a PDMS spacer between a slide glass and a cover glass (Fig. S1, ESI†). A 500 μm-thick sheet of PDMS was made by standard soft lithography, then cut into circular pieces that have the outer and inner diameters, respectively, 25 mm and 22 mm. For injecting liquid and a CO_2 bubble into the Hele-Shaw cell, 1 mm-wide inlet and outlet were made 180° apart from each other. For the Hele-Shaw cell with an inner cell, a circular spacer (PDMS) of 6 mm outer diameter and 4 mm inner diameter was placed concentrically to the outer wall. Then, through the hole on the slide glass, CO_2 is pressurized in the inner cell at a constant pressure (p_1 = 3 psi).

2. CO_2-driven diffusiophoresis of polystyrene particles

A. Particle suspension. Amine-modified polystyrene particles (Sigma Aldrich, diameter = 1 μm, batches MKBX6372V and MKCF6014) were diluted in deionized (DI) water at 0.05 vol%. Polystyrene particles (Thermo Fisher Scientific, diameter = 1 μm) were diluted in DI water at 0.03 vol%.

B. Charged particles near a dissolving CO_2 bubble. In the Hele-Shaw cell shown in Fig. S1(e) (ESI†), a CO_2 bubble is injected to obtain an initial diameter $d_0 \approx$ 5–6 mm. Then with an inverted microscope (Leica DMI4000B), fluorecent images of particles near the moving boundary were taken every 2 seconds.

C. Charged particles near a CO_2-pressurized cell. After the particles were loaded in the chamber between the inner cell and the outer wall (Fig. S1(f), ESI†), gaseous CO_2 was filled in the inner cell and maintained pressurized at p_1 = 3 psi. We fix the starting time of the experiments to be the time point when the valve of CO_2 stream is open. Then with an inverted microscope, fluorescent images of particles near the fixed boundary were taken every 2 seconds.

D. Long-time experiments with a CO_2 bubble. A square Hele-Shaw cell (2 cm × 2 cm) was first filled with the particle suspension (a-PS and PS), then a CO_2 bubble was injected. After ≈20 minutes, the inlet and outlet were sealed with epoxy adhesive to prevent evaporation-driven particle flow. There are always small air bubbles trapped between the liquid phase and the epoxy (in the inlet and outlet), and thus the epoxy was not in contact with the solutions. Photos of the chambers were taken up to 16 hours (ESI,† Section V).

3. CO_2-driven diffusiophoresis of *V. cholerae* cells

A. Bacterial suspension. All *V. cholerae* strains used in this study are derivatives of the wild-type *Vibrio cholerae* O1 biovar El Tor strain C6706.[44] Additional mutations were engineered into this *V. cholerae* strain using *Escherichia coli* S17-*λpir* carrying pKAS32.[45] All *V. cholerae* strains (see ESI† for strain information) were grown overnight at 37 °C in liquid LB with shaking. After 20 hours of growth in LB, the sample was centrifuged at ≈500 × *g* for 7–8 minutes. After removing supernatant, the pellet was resuspended in 5 mL M9 minimal salt solution and allowed to regrow for an additional 2 hours (at 37 °C, with shaking) to achieve exponential phase (OD ≈ 1). Subsequently, for the CO_2-driven diffusiophoresis experiments, the suspension was centrifuged at ≈500 × *g* for 7–8 minutes, and resuspended into 5 mL 10% M9 minimal salt solution to achieve an OD_{600} = 0.23 (Beckman Coulter DU730). A detailed strain list is provided in ESI,† Table S1.

B. *V. cholerae* near a dissolving CO_2 bubble. Similar to the particle experiments, the bacterial suspension was first introduced into the Hele-Shaw cell (Fig. S1(e), ESI†), then a CO_2 bubble (a_0 = 5–6 mm) was injected. Fluorescent images were taken near the bubble interface every 30 minutes.

C. *V. cholerae* near a CO_2-pressurized cell. The Hele–Shaw cell (Fig. S1(f), ESI†) was filled with the *V. cholerae* suspension, and the CO_2 valve was opened. For intensity measurements and PIV, fluorescent images were taken every 5 minutes and every 10 s, respectively.

4. Particle image velocimetry and particle tracking

Micro Particle Image Velocimetry (PIV) was applied to the digital images of fluorescent bacterial cells and PS particles, which were captured every 10 s, with spatial resolution of 0.5 μm per pixel, using the Leica DFC360 FX (mounted on Leica DMI4000B) and a 20× objective. An ensemble cross-correlation scheme was performed using the open source software, JPIV (www.jpiv.vennemann-online.de). For data presented here, square interrogation windows of 128 × 128 pixels with 50% overlap were used to obtain a final vector spacing of 32 μm in the calculated velocity field. Wider interrogation windows were used for analyzing the *P. auruginosa* strain leading to radial vector spacing of 49 μm.

For individual particle tracking, the fluorescent images obtained every 1 second are used. Particle trajectories are obtained with Mosaic Particle Tracker[46] (ImageJ). Trajectories that are longer than 60 frames are chosen for velocity measurements. 1 minite-average of radial velocities are plotted for analysis.

5. CO_2-driven diffusiophoresis of *S. aureus* cells

A. Bacterial suspension. *S. aureus* strains[34] were grown overnight at 37 °C in liquid LB with shaking. After 16–17 hours of growth in LB, the sample was centrifuged at ≈500 × *g* for 7–8 minutes. After removing supernatant, the pellet was resuspended in 5 mL M9 minimal salt solution and allowed to regrow for an additional 2 hours (at 37 °C, with shaking). Then for the CO_2-driven diffusiophoresis experiments, the suspension was centrifuged at ≈500 × *g* for 7–8 minutes, and resuspended into 10% M9 minimal salt solution (after removing supernatant) to achieve an OD_{600} = 0.3.

B. *S. aureus* near a CO_2-pressurized cell. The Hele-Shaw cell (Fig. S1(f), ESI†) was filled with the *S. aureus* suspension, and CO_2 valve was open. For PIV, fluorescent images were taken every 10 seconds.

C. *S. aureus* adhesion to a PDMS substrate. The test chamber was made similar to the Hele-Shaw cell used in the main experiments with a 500 μm PDMS spacer (Fig. S1(e), ESI†), but instead of the slide glass, a 4 mm thick PDMS block was bonded as the bottom substrate (Main text Fig. 5(b-i)). For the scenario in Fig. 5(b-ii), a 1.5–2 mm thick PDMS sheet was used for the bottom substrate, and it was bonded to another circular chamber (diameter ≈ 1 cm, height ≈ 100 μm), which is for pressurizing CO_2. For the third case (Fig. 5(b-iii)), a 4 mm thick, carbonated–water (CW)-saturated (for 24 hours in total, the CW was replaced after 20 hours) PDMS block was bonded as the bottom substrate. Fluorescent images were taken every 10 seconds.

6. CO_2-driven diffusiophoresis of *P. aeruginosa* cells

A. Bacterial suspension. *P. aeruginosa* strains[35] were grown overnight at 37 °C in liquid LB with shaking. After 24–25 hours of growth in LB, the sample was centrifuged at ≈500 × *g* for 7–8 minutes. After removing supernatant, the pellet was resuspended in M9 minimal salt solution and allowed to regrow for an additional 2 hours (at 37 °C, with shaking). Then for the CO_2-driven diffusiophoresis experiments, the suspension was centrifuged at ≈500 × *g* for 7–8 minutes, and resuspended into 10% M9 minimal salt solution (after removing supernatant) to achieve an OD_{600} = 0.3.

B. *P. aeruginosa* near a CO_2-pressurized cell. The Hele–Shaw cell (Fig. S1(f), ESI†) was filled with the *P. aeruginosa* suspension, and CO_2 valve was opened. For PIV, fluorescent images were taken every 10 seconds.

For the long-time experiment, the CO_2 valve was kept open for 1 hour, and fluorescent images were obtained every 5 minutes up to 1 hour. Then the fluorescent images were taken at t = 12 h (11 hours after the CO_2 stream was turned off). For the control experiments without CO_2, fluorescent images were taken at t = 0, 1, and 12 h.

Contributions

S. S. and H. A. S. conceived the project. S. S. designed and performed all experiments. S. K. conducted PIV. S. S., C. Y. L., J. T. A. conducted numerical calculations. J. Y. constructed the *V. cholerae* strains. S. S., B. R., O. S., and H. A. S. set up the theoretical model. All authors contributed to data analysis and writing the paper.

Conflicts of interest

The authors declare no competing financial interests. The corresponding authors have filed a provisional patent application related to this work.

Acknowledgements

We thank the Bassler Lab for providing the *V. cholerae* strains (JY019 and JY238) for the current study. S. S. thanks Minyoung Kim and Christina Kurzthaler for valuable discussions. S. S. and H. A. S. acknowledge the NSF for support *via* CBET-1702693. S. K. thanks LOréal-UNESCO UK and Ireland for support *via* the FWIS 2019 fellowship. J. Y. holds a Career Award at the Scientific Interface from the Burroughs Wellcome Fund.

References

1 R. Rusconi and H. A. Stone, Shear-induced diffusion of platelike particles in microchannels, *Phys. Rev. Lett.*, 2008, **101**, 254502.

2 A. Lenshof and T. Laurell, Continuous separation of cells and particles in microfluidic systems, *Chem. Soc. Rev.*, 2010, **39**, 1203–1217.

3 D. Di Carlo, D. Irimia, R. G. Tompkins and M. Toner, Continuous inertial focusing, ordering, and separation of particles in microchannels, *Proc. Natl. Acad. Sci. U. S. A.*, 2007, **104**(48), 18892–18897.
4 C. Wang, S. V. Jalikop and S. Hilgenfeldt, Efficient manipulation of microparticles in bubble streaming flows, *Biomicrofluidics*, 2012, **6**, 012801.
5 K. L. Kounovsky-Shafer, J. P. Hernandes-Ortiz, K. Potamousis, G. Tsvid, M. Place, P. Ravindran, K. Jo, S. Zhou, T. Odijk, J. J. dePablo and D. C. Schwartz, Electrostatic confinement and manipulation of DNA molecules for genome analysis, *Proc. Natl. Acad. Sci. U. S. A.*, 2017, **114**(51), 13400–13405.
6 X. Hu, P. H. Bessette, J. Qian, C. D. Meinhart, P. S. Daugherty and H. T. Soh, Marker-specific sorting of rare cells using dielectrophoresis, *Proc. Natl. Acad. Sci. U. S. A.*, 2005, **102**(44), 15757–15761.
7 S. Shim, *Interfacial Flows with Heat and Mass Transfer*, PhD thesis, Princeton Univ., 2017.
8 J. Palacci, B. Abécassis, C. Cottin-Bizonne, C. Ybert and L. Bocquet, Colloidal motility and pattern formation under rectified diffusiophoresis, *Phys. Rev. Lett.*, 2010, **104**, 138302.
9 D. C. Prieve, J. L. Anderson, J. P. Ebel and M. E. Lowell, Motion of a particle generated by chemical gradients. Part 2. Electrolytes, *J. Fluid Mech.*, 1984, **148**, 247–269.
10 D. Florea, S. Musa, J. M. R. Huyghe and H. M. Wyss, Long-range repulsion of colloids driven by ion exchange and diffusiophoresis, *Proc. Natl. Acad. Sci. U. S. A.*, 2014, **111**, 6554–6559.
11 S. Shin, O. Shardt, P. B. Warren and H. A. Stone, Membraneless water filtration using CO_2, *Nat. Commun.*, 2017, **8**, 15181, DOI: 10.1038/ncomms15181.
12 D. Velegol, A. Garg, R. Guha, A. Kar and M. Kumar, Origins of concentration gradients for diffusiophoresis, *Soft Matter*, 2016, **12**, 4686–4703.
13 S. V. Hartman, B. Božič and J. Derganc, Migration of blood cells and phospholipid vesicles induced by concentration gradients in microcavities, *New Biotechnol.*, 2018, **47**, 60–66.
14 A. Kar, T.-Y. Chiang, I. O. Rivera, A. Sen and D. Velegol, Enhanced transport into and out of dead-end pores, *ACS Nano*, 2015, **9**, 746–753.
15 S. Shin, E. Um, B. Sabass, J. T. Ault, M. Rahimi, P. B. Warren and H. A. Stone, Size-dependent control of colloid transport via solute gradients in dead-end channels, *Proc. Natl. Acad. Sci. U. S. A.*, 2016, **113**(2), 257–261.
16 N. Shi, R. Nery-Azevedo, A. I. Abdel-Fattah and T. M. Squires, Diffusiophoretic focusing of suspended colloids, *Phys. Rev. Lett.*, 2016, **117**, 258001.
17 A. Banerjee, I. Williams, R. N. Azevedo, M. E. Helgeson and T. M. Squires, Soluto-inertial phenomena: Designing long-range, long-lasting, surface-specific interactions in suspensions, *Proc. Natl. Acad. Sci. U. S. A.*, 2016, **113**(31), 8612–8617.
18 A. Kar, R. Guha, N. Dani, D. Velegol and M. Kumar, Particle deposition on microporous membranes can be enhanced or reduced by salt gradients, *Langmuir*, 2014, **30**, 793–799.
19 R. Guha, X. Shang, A. L. Zydney, D. Velegol and M. Kumar, Diffusiophoresis contributes significantly to colloidal fouling in low salinity reverse osmosis systems, *J. Membr. Sci.*, 2015, **479**, 67–76.
20 W. W. Wilson, M. M. Wade, S. C. Holman and F. R. Champlin, Status of methods for assessing bacterial cell surface charge properties based on zeta potential measurements, *J. Microbiol. Methods*, 2001, **43**, 153–164.
21 E. Kłodzińska, M. Szumski, E. Dziubakiewicz, K. Hrynkiewicz, E. Skwarek, W. Janusz and B. Buszewski, Effect of zeta potential value on bacterial behavior during electrophoretic separation, *Electrophoresis*, 2010, **31**, 1590–1596.
22 S. Shim, J. Wan, S. Hilgenfeldt, P. D. Panchal and H. A. Stone, Dissolution without disappearing: multicomponent gas exchange for CO_2 bubbles in a microfluidic channel, *Lab Chip*, 2014, **14**, 2428–2436.
23 P. Peñas-López, M. A. Parrales and J. Rodriguez-Rodriguez, Dissolution of a CO_2 spherical cap bubble adhered to a flat surface in air-saturated water, *J. Fluid Mech.*, 2015, **775**, 53–76.
24 P. Peñas-López, B. van Elburg, M. A. Parrales and J. Rodríguez-Rodríguez, Diffusion of dissolved CO_2 in water propagating from a cylindrical bubble in a horizontal Hele–Shaw cell, *Phys. Rev. Fluids*, 2017, **2**, 063602.
25 W. M. Haynes, *CRC Handbook of Chemistry and Physics*, CRC Press, 96th edn, 2015.
26 B. V. Derjaguin and M. V. Golovanov, On long-range forces of repulsion between biological cells, *Prog. Surf. Sci.*, 1992, **40**, 210–217.
27 T. Fukuyama, A. Fuke, M. Mochizuki, K. Kamei and Y. T. Maeda, Directing and boosting of cell migration by the entropic force gradient in polymer solution, *Langmuir*, 2015, **31**, 12567–12572.
28 Y. Cheng and C. I. Moraru, Long-range interactions keep bacterial cells from liquid-solid interfaces: evidence of bacteria exclusion zone near Nafion surfaces and possible implications for bacterial attachment, *Colloids Surf., B*, 2018, **162**, 16–24.
29 H. Lee, J. Kim, J. Yang, S. W. Seo and S. J. Kim, Diffusiophoretic exclusion of colloidal particles for continuous water purification, *Lab Chip*, 2018, **18**, 1713–1724.
30 S. Karasawa, T. Araki, T. Nagai, H. Mizuno and A. Miyawaki, Cyan-emitting and orange-emitting fluorescent proteins as a donor/acceptor pair for fluorescence resonance energy transfer, *Biochem. J.*, 2004, **381**, 307–312.
31 S. Kabir and S. Ali, Characterization of surface properties of *Vibrio cholerae*, *Infect. Immun.*, 1983, **39**, 1048–1058.
32 T. Vissers, A. T. Brown, N. Koumakis, A. Dawson, M. Hermes, J. Schwarz-Linek, A. B. Schofield, J. M. French, V. Koutsos, J. Arlt, V. A. Martinez and W. C. K. Poon, Bacteria as living patchy colloids: phenotype heterogeneity in surface adhesion, *Sci. Adv.*, 2018, **4**, eaao1170.
33 A. Gupta, S. Shim, L. Issah, C. McKenzie and H. A. Stone, Diffusion of multiple electrolytes cannot be treated independently: Model predictions with experimental validation, *Soft Matter*, 2019, **15**, 9965–9973.

34 S. Khodaparast, M. K. Kim, J. E. Slipe and H. A. Stone, Bubble-driven detachment of bacteria from confined microgeometries, *Environ. Sci. Technol.*, 2017, **51**, 1340–1347.

35 A. Siryaporn, M. K. Kim, Y. Shen, H. A. Stone and Z. Gitai, Colonization, competition, and dispersal of pathogens in fluid flow networks, *Curr. Biol.*, 2015, **25**, 1201–1207.

36 S. Halder, K. K. Yadav, R. Sarkar, S. Mukherjee, P. Saha, S. Haldar, S. Karmakar and T. Sen, Alteration of zeta potential and membrane permeability in bacteria: a study with cationic agents, *SpringerPlus*, 2015, **4**, 672.

37 L.-A. B. Rawlinson, J. P. O'Gara, D. S. Jones and D. J. Brayden, Resistance of *Staphylococcus aereus* to the cationic antimicrobial agent poly(2-(dimethylamino ethyl)-methacrylate) (pDMAEMA) is influenced by cell-surface charge and hydrophobicity, *J. Med. Microbiol.*, 2011, **60**, 968–976.

38 J. Shephard, A. J. McQuillan and P. J. Brenner, Mechanisms of cation exchange by *Pseudomonas aeruginosa* PAO1 and PAO1 *wbpL*, a strain with a truncated lipopolysaccharide, *Appl. Environ. Microbiol.*, 2008, **74**, 6980–6986.

39 T. J. Foster and M. Höök, Surface protein adhesins of Staphylococcus aureus, *Trends Microbiol.*, 1998, **6**, 485–488.

40 A. Gupta, S. Shim and H. A. Stone, DIffusiophoresis: from dilute to concentrated electrolytes, *Soft Matter*, 2020, **16**, 6975–6984.

41 S. W. Joo, S. Y. Lee, J. Liu and S. Qian, Diffusiophoresis of an elongated cylindrical nanoparticle along the axis of a nanopore, *ChemPhysChem*, 2010, **11**, 3281–3290.

42 K. D. Mena and C. P. Gerba, Risk assessment of pseudomonas aeruginosa in water, *Rev. Environ. Contam. Toxicol.*, 2009, **201**, 71–115.

43 M. Shigematsu, Y. Meno, H. Misumi and K. Amako, The measurement of swimming velocity of *Vibrio cholerae* and *Pseudomonas aeruginosa* using the video tracking method, *Microbiol. Immunol.*, 1995, **39**, 741–744.

44 K. H. Thelin and R. K. Taylor, Toxin-coregulated pilus, but not mannose-sensitive hemagglutinin, is required for colonization by *V. cholerae* O1 El Tor biotype and O139 strains, *Infect. Immun.*, 1996, **64**, 2853–2856.

45 K. Skorupski and R. K. Taylor, Positive selection vectors for allelic exchange, *Gene*, 1996, **169**, 47–52.

46 I. F. Sbalzarini and P. Koumoutsakos, Feature point tracking and trajectory analysis for video imaging in cell biology, *J. Struct. Biol.*, 2005, **151**, 182–195.